Enhanced photoluminescence emission from bandgap shifted InGaAs/InGaAsP/InP microstructures processed with UV laser quantum well intermixing

2013 J. Phys. D: Appl. Phys. 46 445103

(http://iopscience.iop.org/0022-3727/46/44/445103)

IOP Publishing Journal of Physics D: Applied Physics
J. Phys. D: Appl. Phys. **46** (2013) 445103 (7pp) doi:10.1088/0022-3727/46/44/445103

Enhanced photoluminescence emission from bandgap shifted InGaAs/InGaAsP/InP microstructures processed with UV laser quantum well intermixing

Neng Liu[1], **Suzie Poulin**[2] **and Jan J Dubowski**[1,3]

[1] Laboratory for Quantum Semiconductors and Photon-based BioNanotechnology, Regroupement québécois sur les matériaux de points (RQMP), Interdisciplinary Institute for Technological Innovation (3IT), Faculty of Engineering, Université de Sherbrooke, Sherbrooke, Québec J1K 2R1, Canada
[2] Laboratory for Material Surface Analysis, École Polytechnique de Montréal, Québec H3T 1J4, Canada

E-mail: jan.j.dubowski@usherbrooke.ca

Received 30 June 2013, in final form 4 September 2013
Published 16 October 2013
Online at stacks.iop.org/JPhysD/46/445103

Abstract
In spite of many years of research, the quantum well intermixing technique has not been able to deliver multibandgap III–V semiconductor wafers at highly attractive costs. We report that UV laser irradiation of InGaAs/InGaAsP/InP quantum well (QW) microstructures in deionized water and rapid thermal annealing (RTA) allows achieving, mask-free, wafers with blueshifted photoluminescence (PL) emission of intensity exceeding almost 10× that of the RTA-only wafers. Our calculations indicate that a ∼40 nm thick InO_x layer formed on top of the investigated microstructure induces compressive strain in the QW region and leads to this record-high enhanced PL amplitude.

(Some figures may appear in colour only in the online journal)

The selective area control of the bandgap of semiconductor wafers is one of the key factors in the development of photonic integrated circuits (PICs) (Estrella *et al* 2012). Post-growth quantum well intermixing (QWI) has been reported as a relatively simple and potentially cost-effective method allowing area-selective bandgap tuning of $Si/Si_{1-x}Ge_x$ (Dubowski *et al* 1999) and III–V quantum well (QW) wafers (Skogen *et al* 2005, Genest *et al* 2008, Xu and Mei 2009, Coldren *et al* 2011) (and references therein). The quality of the QWI material has frequently been investigated with the photoluminescence (PL) effect. Examples of such studies include material fabricated with ion implantation induced disordering (Elman *et al* 1989, Jie *et al* 2006), sputtered SiO_2 intermixing (McDougall *et al* 1998), Ar ion plasma (Djie *et al* 2003, Nie *et al* 2006), SiO_2/Si_xN_y cap layers (Teng *et al* 2002, Francois *et al* 2006), and both IR (Dubowski *et al* 2002, Stanowski and Dubowski 2009) and UV laser (Dubowski 2003, Genest *et al* 2007b) induced intermixing. The quality of the QWI material has also been investigated with Raman spectroscopy (Ong *et al* 2000, Helmy *et al* 2006), secondary ion mass spectroscopy (SIMS) (Teng *et al* 2002) as well as with devices, such as waveguides (Haysom *et al* 1999) and laser diodes (Noel *et al* 1996, Paquette *et al* 1997, Dubowski *et al* 2002). Numerous results have reported some degradation of the optical properties of QWI material manifested, e.g., by reduced QW PL intensity (Jie *et al* 2006) and increased both waveguide losses (Haysom *et al* 1999) and laser threshold current (Dubowski *et al* 2002). While reduced quantum confinement could account for some of these changes, an excessive uptake of impurities from the processing environment has often contributed to the increased intermixing amplitude and reduced device performance. The surface damage of InP cap and formation of defects propagating deep into the active region could lead to

[3] Author to whom any correspondence should be addressed.
URL: www.dubowski.ca

significantly decreased PL signals (McDougall *et al* 1998, Jie *et al* 2006). However, a 1.9× enhanced PL intensity has been reported for a lattice-matched Zn-doped InGaAs/InGaAsP/InP microstructure blueshifted with Ar plasma by 86 nm (Djie *et al* 2003), while the same technique applied to a lattice-matched undoped InGaAs/InGaAsP/InP microstructure, produced a 16 nm blueshifted material emitting PL reduced by 50% (Nie *et al* 2006). The importance of a processing environment on the quality of the QWI material has been illustrated with a variety of proximity caps employed during rapid thermal annealing (RTA), indicating that annealing with a Si proximity cap could produce a 90 nm blueshifted InGaAs/InGaAsP material emitting PL signal 2× more intense than that from the material capped with an InP proximity cap (Hulko *et al* 2006).

We have employed a UV laser QWI technique for processing of III–V QW microstructures (Dubowski 2003), and we have demonstrated large bandgap blueshifts ($\Delta\lambda \sim 130$ nm) in InGaAs/InGaAsP/InP microstructures (Genest *et al* 2008, Liu and Dubowski 2013), while significant inhibition of the intermixing effect in AlGaAs/GaAs and InAlGaAs/AlGaAs/GaAs microstructures (Genest *et al* 2007a, Genest *et al* 2007b). The irradiation experiments with both 193 and 248 nm excimer lasers carried out for samples surrounded by atmospheric air (Genest *et al* 2007a, 2007b, Genest *et al* 2008), deionized water (Liu and Dubowski 2013), SiO_x (Liu *et al* 2012) and SiN_x (Liu *et al* 2010) environments have clearly demonstrated a dependence of both blueshifting and QW PL intensity on those environments. For instance, in comparison to the intensity of the RTA only material, a 2× enhanced QW PL intensity has been observed in the lattice-matched material irradiated in air with an ArF laser and blueshifted by 74–83 nm (Genest *et al* 2008). Recently, a 1.4× PL intensity enhancement has been reported in a 140 nm blueshifted, compressively strained (∼1%), InGaAsP/InGaAsP/InP QW heterostructure irradiated in air with a KrF laser (Kaleem *et al* 2013).

The presence of excessive impurities in the proximity of the QW region, while promoting the QWI effect, could be the source of the reduced amplitude of the QW PL emission due to increased non-radiative recombinations. This effect would intensify in microstructures with the surface-QW distance significantly reduced from its typical 1–2 μm used in laser microstructures. We addressed this issue by investigating the origin of enhanced PL emission in InGaAs/InGaAsP/InP QW microstructure with the active region located approximately 80 nm below the surface.

A cross-section of the investigated InGaAs/InGaAsP/InP microstructure is shown in figure 1. The microstructure, grown on S-doped InP (0 0 1) substrate, consists of five (5) 6 nm thick $In_{0.32}Ga_{0.68}As$ QW separated by four (4) 10 nm-thick $In_{0.79}Ga_{0.21}As_{0.42}P_{0.58}$ barriers. The QW stack is under a nominal 0.8% compressive strain induced by the difference in chemical compositions of barriers and wells. The microstructure comprises 110 and 20 nm thick InGaAsP graded bandgap layers, designed to provide optical waveguiding. They interface the QW stack from the substrate and surface sides, respectively. The microstructure is interfaced with a 40 nm thick InP and a 6 nm thick

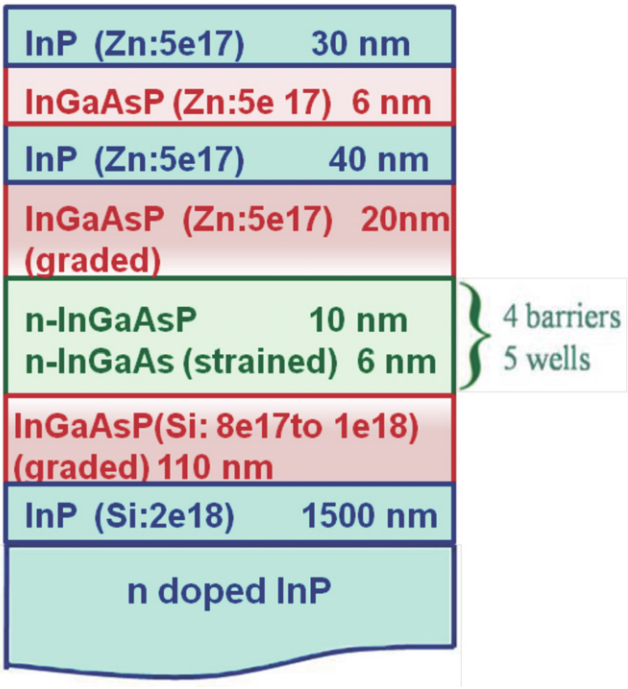

Figure 1. A cross-section of the investigated InGaAs/InGaAsP QW microstructure.

etch-stop InGaAsP layer and, finally, capped with a 30 nm thick InP layer. The top contact and active regions of the microstructure were Zn-doped at 5×10^{17} cm^{-3} and 8×10^{17} cm^{-3}, respectively. The microstructure was designed to emit PL at 1540 nm at room temperature.

The samples of 10 mm × 10 mm dimensions, following their degreasing in Opticlear, acetone, and isopropyl alcohol, were installed in a 0.74 mm tall Teflon chamber covered with a fused silica window. The chamber was filled with an atmospheric pressure air or DI water and the irradiation was carried out with an ArF-based projection system described elsewhere (Liu and Dubowski 2013). A series of 0.9 mm diameter sites were irradiated on each sample, nominally under identical condition, with pulse fluence of 82 mJ cm^{-2}. The irradiated samples prepared for surface analyses were stored immediately in a N_2 filled box that provided protection against air oxidation. The RTA step was carried out at 700 °C for 2 min in a forming gas environment ($N_2 : H_2 = 9 : 1$) using a commercial furnace (JIPELEC, Jetfirst). During RTA, the samples were installed face down on a silicon wafer employed as a capping material.

The PL signal from processed samples was collected at room temperature with a commercial PL mapper (Philips, PLM-150) equipped with an Nd : YAG laser ($\lambda = 1.06\,\mu$m) excitation source.

The surface chemical modification was investigated with an x-ray photoelectron spectroscopy (XPS) (AXIS Ultra DLD, Kratos Analytical). The analysis was carried out with a take-off-angle normal to the sample surface. The high-resolution scans of analysed areas, typically 220 μm × 220 μm, were observed in constant energy modes with a 20 eV pass energy filter. To compensate the surface charging effect, all XPS data binding energies (BEs) were referenced to the adventitious C

1s peak at the BE of 285.0 eV. Quantification of XPS data was carried out using Casa XPS software as detailed in our previous work (Liu and Dubowski 2013).

Atomic depth profiling was investigated with a time-of-flight SIMS instrument (ToF-SIMS IV, IONTOF) operating at a base pressure of 3×10^{-9} Torr. A sample area of 500 μm × 500 μm was sputtered with a 3 keV Cs ion source at an approximate rate of 0.08 nm s^{-1}. A central area of 50 μm × 50 μm from the sputtered region was probed with a 10 keV Bi ion beam.

The ArF laser irradiation of InP, due to the relatively strong absorption of the 193 nm radiation (6.4 eV), initially modifies an approximately 8 nm deep layer (Aspnes and Studna 1983, Liu *et al* 2012). The RTA activated processes and diffusion modify the chemical composition of that layer and further increase its thickness. The PL shift and intensity of excimer laser irradiated QW microstructures was reported to be affected by the surface chemical state and morphology (Dubowski *et al* 1999, Liu *et al* 2012), but the mechanism of this enhancement has remained relatively unknown. Figure 2 compares PL spectra from as-grown material before and after RTA with those from the sites irradiated with the laser in air and in DI water (figures 2(*a*) and (*b*), respectively). The insets are PL intensity maps of the samples displaying the sites irradiated with the indicated pulse number and annealed in an RTA furnace. The colour scale bars on the right provide a reference to the measured PL intensities. While RTA of the as-grown material blueshifts its PL emission by about 15 nm, the irradiation in air with 20 pulses and RTA lead to the fabrication of the QWI material net blueshifted by 72 nm. This compares to the material net blueshifted by only 32 nm that was irradiated in DI water with the same laser parameters (pulse number and fluence). The greater blueshift of the site irradiated in air must be due to the excessive contribution from impurities and/or laser-induced modification of the surface. This is consistent with drastically decreased PL intensities observed from all sites irradiated in air. In contrast, significantly increased PL peak intensities have been measured from the sites irradiated in water. For instance, the 20-pulse irradiated site, blueshifted by 32 nm, emits PL signal at 2300 c.u., which is 2.1× more intense than that of the as-grown material, and 9× more intense than the PL signal of the RTA-only material.

AFM data revealed only minimal surface roughening of the sites irradiated in air and DI water. The 50-pulse irradiated sites exhibited $\sigma_{RMS} \sim 6$ nm (compared to $\sigma_{RMS} \sim 1$ nm for the as-grown material) that was reduced to $\sigma_{RMS} \sim 3.2$ nm after the RTA step. Thus the PL intensity enhancement due to surface nanostructurization is negligible in our samples. The PL full-width at half-maximum (FWHM) (PL_{FWHM}) of the as-grown material was reduced from 82 nm to 77–75 nm after RTA. The PL_{FWHM} of 77 nm was observed for the sites irradiated with 20 pulses in DI H_2O (following the RTA step), while the sites irradiated with the same number of pulses in air exhibited PL_{FWHM} increased to 84 nm. The irradiation with 50 pulses in DI H_2O produced a material with $PL_{FWHM} \approx 82$ nm, i.e., comparable to that of the as-grown material. This suggests that no significant deterioration of the active region is induced by the laser irradiation in DI H_2O.

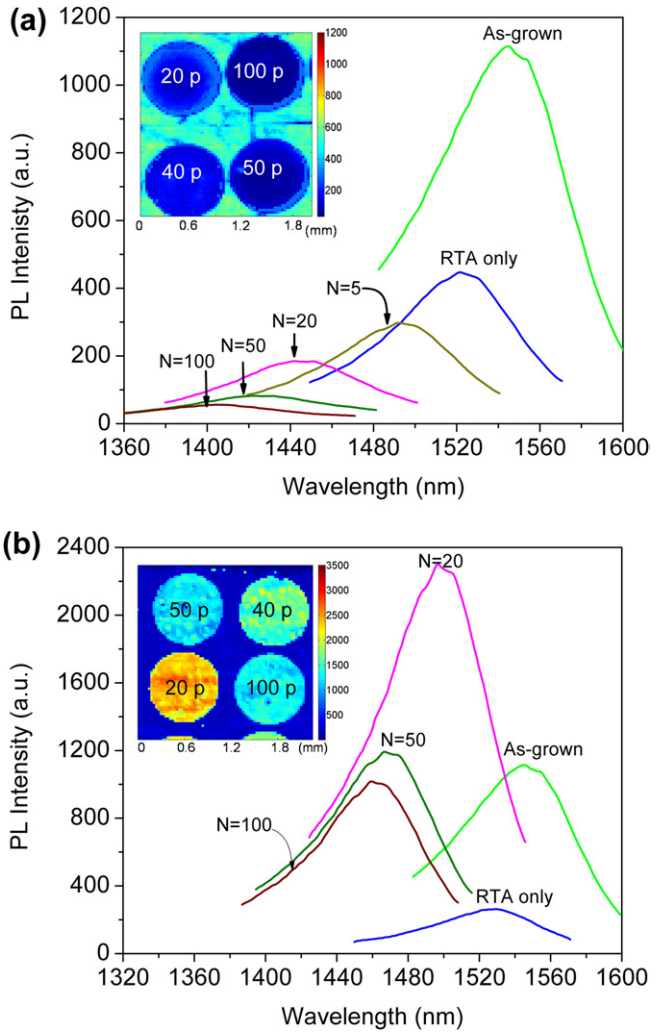

Figure 2. PL spectra of as-grown material and sites irradiated in air (*a*) and DI water (*b*) following the RTA step. The insets are PL intensity maps of the samples displaying the sites irradiated with the indicated pulse number and annealed in an RTA furnace.

To investigate the feasibility of a compressive strain increased PL emission intensity due to increased splitting energy between the heavy and light hole bands (Tsuchiya *et al* 1994), we studied the chemical composition of the investigated samples using XPS and ToF-SIMS. Figure 3 shows the In $3d_{5/2}$ XPS spectra of sites irradiated with 50 pulses of the ArF laser at 82 mJ cm^{-2} in air and DI water before (figures 3(*a*) and (*c*)) and after the RTA step (figures 3(*b*) and (*d*)). A massive amount of InP_xO_y (including $In(PO_3)_3$, $In_y(PO_4)$, $In(PO_3)_x$ and InO_x) can be seen on the sample irradiated in air. In contrast, a significantly smaller amount of InP_xO_y has been observed on the sample irradiated in DI water. The formation of a significantly InP_xO_y-enriched surface seems to be related to the availability of excessive oxygen as well as to a greater surface temperature induced with the laser irradiating the sample in air (Liu and Dubowski 2013).

For the sample irradiated in air, the P/In ratio decreases to 0.8 as the pulse number increases to 50 pulses. A similar P/In ratio was observed in InP capped QW microstructure during argon-plasma induced QWI (Xu and Mei 2009). Since

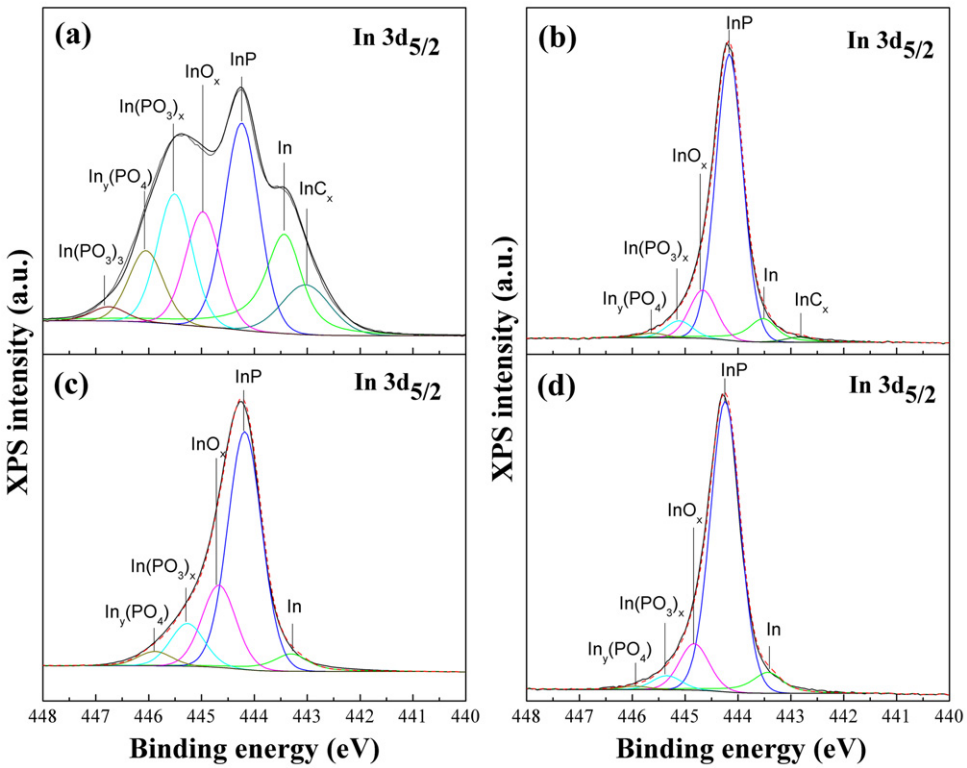

Figure 3. In $3d_{5/2}$ XPS spectra of sample irradiated by ArF laser at 82 mJ cm^{-2} with 50 pulses in air (*a*), (*b*) and DI water (*c*), (*d*) before (*a*), (*c*) and after (*b*), (*d*) RTA.

Table 1. XPS P/In ratio in the as-grown InP-covered InGaAs/InGaAsP/InP microstructure and ArF irradiated sites before RTA.

	Non-irradiated	20 pulses	50 pulses	100 pulses
In DI water	1.0	1.1	1.2	1.1
In air	1.0	0.9	0.8	0.8

Table 2. XPS P/In ratio in the as-grown InP-covered InGaAs/InGaAsP/InP microstructure and ArF irradiated sites after 2 min RTA at 700 °C.

	Non-irradiated	20 pulses	50 pulses	100 pulses
In DI water	1.1	1.0	1.0	1.0
In air	1.1	1.1	1.1	1.1

the preferential sputtering of P leads to the formation of P vacancies or In interstitials, enhanced intermixing could be expected in such a case (Genest *et al* 2008, Xu and Mei 2009). In contrast, the P/In ratio for the 50-pulse site irradiated in DI water increased by 20%. The preferential loss of In in samples UV laser irradiated in DI water, with P/In ratio of ∼1.2 and excessive formation of P–P surface clusters, has been reported in the literature (Kumar and Soni 2010). This behaviour could be traced to the lower surface temperature of InP irradiated in water versus that irradiated in air for comparable laser parameters (Zimmerman *et al* 1991). During RTA, the excessive P atoms diffuse into the microstructure and contribute to the formation of interstitial defects via the kick out mechanism as observed, e.g., in InP-based QW microstructures coated with a low-temperature deposited P-rich InP cap layer (Hulko *et al* 2006). Tables 1 and 2 summarize the XPS results concerning the P/In ratio observed for the investigated samples before and after the RTA step, respectively.

It can be seen that, following the RTA step, the stoichiometry of the InP surface, averaged over the XPS probing depth (∼10 nm), has been restored for the samples irradiated in DI water. In contrast, the stoichiometric InP surface of non-irradiated microstructures, as well as the P-deficient surface of samples irradiated in air become P-rich due to outdiffusion of this element during the RTA step.

Figure 4 compares ToF-SIMS profiles of phosphorus (P^-) (——), arsenic (As^-) (——), oxygen (O^-) (- - - -), and InO^- (——) ions in as-grown material and the 50-pulse material irradiated in air and DI water, all after RTA. We note that InO^- is the main component (∼80%) of all the In-oxides (InO_2^-, $In_2O_3^-$) observed with ToF-SIMS. The P^- intensity profile in the RTA-only sample (figure 4(*a*)) is followed by the weak intensity profile of O^- that follows relatively well the structural composition of the active region. As a reference, the O^- ion signal above 100 counts s^{-1} is observed in the top 20 nm thick portion of the microstructure. Our results are consistent with the presence of O reported in MBE (Achtnich *et al* 1987) and MOCVD (Sugg *et al* 1993) grown P-based QW microstructures due to a relatively strong reactivity of P (Xiang *et al* 2001). A significantly increased concentration of O^- observed in figure 4(*b*) illustrates an efficient uptake O from air. The O^- ion intensity in this case drops to below 100 counts s^{-1} only after about 100 nm of the material has been

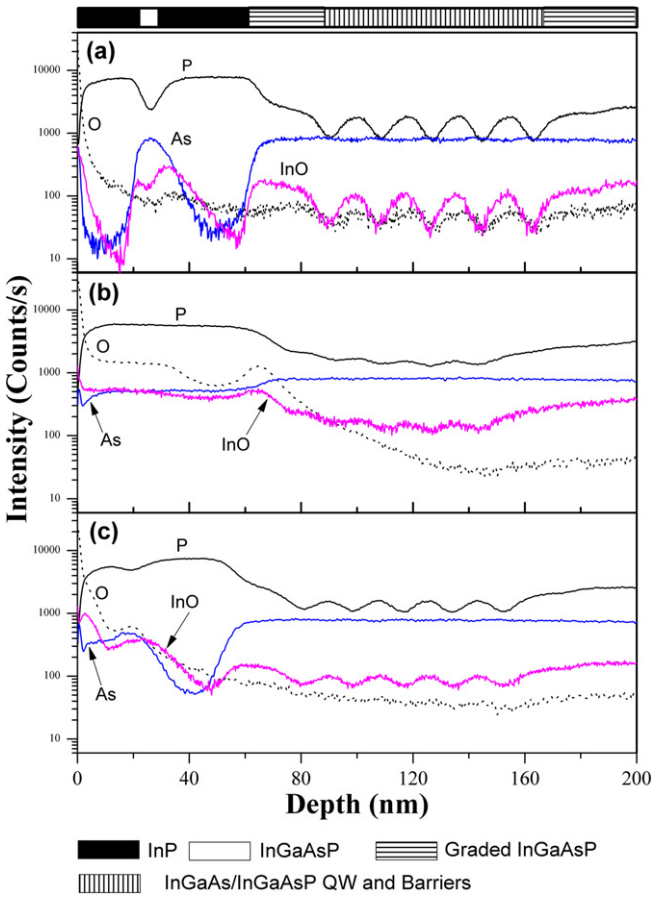

Figure 4. P (——), O (- - - -), As (——) and InO (——) intensity profiles in the microstructure after RTA of as-grown sample (*a*) and samples irradiated by ArF laser at 82 mJ cm^{-2} with 50 pulses in air (*b*) and DI water (*c*) investigated by ToF-SIMS.

removed. In contrast, O^- signal drops to below 100 counts s^{-1} after about 50 nm removal of the material irradiated in DI water (figure 4(*c*)). Diminishing amplitude of the P^- ion profile in the active region irradiated in air (figure 4(*b*)) illustrates the presence of significant intermixing. The disappearance of the P^- ion minimum related to the presence of the 6 nm thick etch stop InGaAsP layer, originally observed in figure 4(*a*), is also an indication of the strong intermixing phenomenon, although slightly reduced depth resolution is expected during sputtering in ToF-SIMS. In contrast, the presence of the etch-stop layer and four (4) InGaAsP barriers are clearly observed in the sample irradiated in DI water (figure 4(*c*)).

Both XPS and ToF-SIMS results confirm the presence of InO_x at significant concentration in the top portion of the investigated material. InO^- profile in the RTA only sample oscillates around 60 counts s^{-1}, and it increases to ~500 counts s^{-1} at the surface of that sample. This is consistent with the XPS data that revealed InO_x^- as a major component on the surface of RTA samples (see figure 3). For the sample irradiated in air, almost constant InO^- ion intensity at 450 counts s^{-1} is observed in the top 70 nm thick layer, while in the active region, it drops to near 100 counts s^{-1}. The intensity of InO^- ion profile in the active region of the sample irradiated in DI water is slightly below 100 counts s^{-1}, while a compositional gradient of this material is observed over

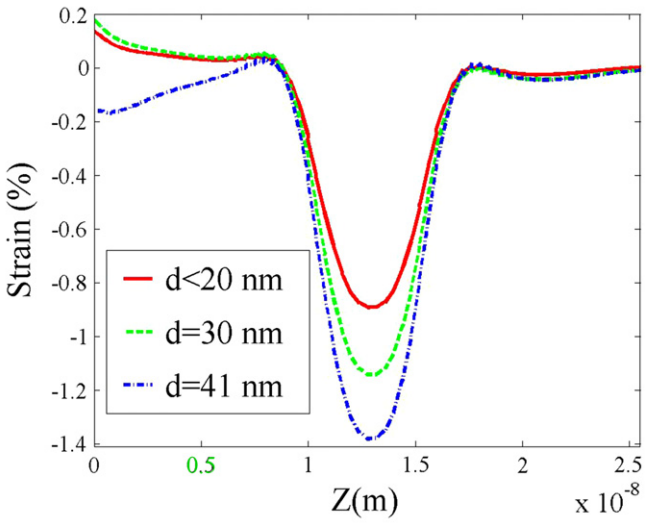

Figure 5. Calculated strain dependence in the 32 nm blueshifted InGaAs/InGaAsP QW region on the thickness, d, of the InO_x stressing layer.

the 70 nm distance, as indicated by the signal increasing from 100 to 800 counts s^{-1} at the surface. Thus, it is clear that the top layer of the investigated material consists of the In–P–O mixture, with InO_x dominating its composition.

We have investigated the role of InO_x on the strain induced in the active region. As the atomic radius of O (60 pm) is smaller than P (100 pm), InO_x has a greater coefficient of thermal expansion (CTE): 10.1×10^{-6} K^{-1} than that of InP: 4.1×10^{-6} K^{-1} (Singh and Shewchun 1978). Thus, in the In–P–O mixed compound, CTE is supposed to increase with increasing concentration of InO_x. The thermal strain from the capped stressor layer on the QW microstructure is defined as (Francois *et al* 2006):

$$\varepsilon = (\alpha_{\text{structure}} - \alpha_{\text{stressor}})\Delta T, \quad (1)$$

where $\alpha_{\text{structure}}$ and α_{stressor} is CTE of the microstructure and the stressor, respectively, and ΔT is the difference between the RTA (700 °C) and room (25 °C) temperatures. The negative value of ε indicates a compressive strain. We assumed that the top 76 nm thick layer consists of an interdiffused $In_xGa_{1-x}As_yP_{1-y}$ and an InO_x cap layer of thickness d that was used as a parameter in COMSOL calculations. The interdiffused composition profile was calculated based on the PL determined blueshift. Figure 5 shows the dependence of the calculated strain in the active region of the microstructure blueshifted by 32 nm on the thickness of the InO_x layer. Note that $z = 0$ in that figure indicates the location of the barrier material above the uppermost QW interfacing the 20 nm thick $In_xGa_{1-x}As_yP_{1-y}$ graded bandgap layer. No significant modification of the strain is observed for $d <$ 20 nm. As the InO_x thickness increases to 41 nm, the compressive strain in the QW region increases to almost 1.4%. It was reported that the PL intensity in InGaAsP/InGaAsP QW microstructures could increase by almost 10 times if the compressive strain in the active region increased from 0.8% to 1.4% (Tsuchiya *et al* 1994). Thus, the amplitude of

PL enhancement observed in our samples is consistent with these calculations. It is feasible that InO_x nanocrystallites could form in the InGaAsP matrix at depths exceeding 40 nm and, thus, contribute to the strain in the active region of conventional laser microstructures. Nevertheless, we argue that the principal source of the PL intensity enhancement observed in the investigated microstructures is strain induced by the InO_x layer.

In summary, the ability to fabricate high-quality QWI material, illustrated by high-intensity QW PL and, e.g., low-threshold laser current fabricated from the QWI material, is critically important for the advancement of the QWI technology and fabrication of PICs. We have employed the UV laser QWI technique that allows eliminating parasitical contribution to QWI by surface-accumulated impurities. An almost ten times more intense PL signal was observed from the 32 nm net blueshifted material in comparison to the RTA-only material. The XPS results indicate that the stoichiometry of the InP surface irradiated in DI water has been restored after the RTA step. This could contribute to some enhancement of the PL signal due to reduced concentration of the surface non-radiative recombination centres. However, our investigations point to the increased strain in the QW region as the leading mechanism responsible for enhanced PL intensity in QWI InGaAs/InGaAsP/InP microstructures. The calculations indicate that a 41 nm thick layer of InO_x formed during RTA of the sample laser irradiated in DI H_2O is a source of the observed effect of PL enhancement. These results demonstrate the potential of the UV laser QWI technique in designing experimental conditions attractive for the fabrication of the QWI material with unique optical and electrical characteristics.

Acknowledgments

This work was supported by the Natural Science and Engineering Research Council of Canada (Discovery Grant No. 122795-2010) and the programme of the Canada Research Chair in Quantum Semiconductors. Technical assistance of the technical staff of the Université de Sherbrooke Centre de recherche en nanofabrication et en nanocaractérisation (CRN^2) is greatly appreciated. NL acknowledges the Merit Scholarship Programme for Foreign Student, Fonds de recherche du Québec-Nature et technologies, for providing a graduate student scholarship.

References

Achtnich T, Burri G, Py M and Ilegems M 1987 Secondary ion mass spectrometry study of oxygen accumulation at GaAs/AlGaAs interfaces grown by molecular beam epitaxy *Appl. Phys. Lett.* **50** 1730–2

Aspnes D E and Studna A A 1983 Dielectric functions and optical parameters of Si, Ge, GaP, GaAs, GaSb, InP, InAs, and InSb from 1.5 to 6.0 eV *Phys. Rev.* B **27** 985–1009

Coldren L A, Nicholes S C, Johansson L, Ristic S, Guzzon R S, Norberg E J and Krishnamachari U 2011 High performance InP-based photonic ICs-A tutorial *J. Light. Technol.* **29** 554–70

Djie H S, Mei T and Arokiaraj J 2003 Photoluminescence enhancement by inductively coupled argon plasma exposure for quantum-well intermixing *Appl. Phys. Lett.* **83** 60–2

Dubowski J J 2003 Laser-induced bandgap shifting for photonic device integration. Laser-induced bandgap shifting for photonic device integration *US Patent* # 6,514,784, CA 2,331,567

Dubowski J J, Feng Y, Poole P, Buchanan M, Poirier S, Genest J and Aimez V 2002 Monolithic multiple wavelength ridge waveguide laser array fabricated by Nd : YAG laser-induced quantum well intermixing *J. Vac. Sci. Technol.* A **20** 1426–9

Dubowski J J, Rowell N, Aers G C, Lafontaine H and Houghton D C 1999 Laser-induced selective area band-gap tuning in $Si/Si_{1-x}Ge_x$ microstructures *Appl. Phys. Lett.* **74** 1948–50

Elman B, Koteles E S, Melman P and Armiento C A 1989 GaAs/AlGaAs quantum-well intermixing using shallow ion-implantation and rapid thermal annealing *J. Appl. Phys.* **66** 2104–7

Estrella S B, Johansson L A, Masanovic M L, Thomas J A and Barton J S 2012 Widely tunable compact monolithically integrated photonic coherent receiver *IEEE Photon. Technol. Lett.* **24** 365–7

Francois A, Aimez V, Beauvais J, Gendry M and Regreny P 2006 Enhancement of quantum well intermixing on InP/InGaAs/InGaAsP heterostructures using titanium oxide surface stressors to induce forced point defect diffusion *Appl. Phys. Lett.* **89** 164107

Genest J, Beal R, Aimez V and Dubowski J J 2008 ArF laser-based quantum well intermixing in InGaAs/InGaAsP heterostructures *Appl. Phys. Lett.* **93** 071106

Genest J, Dubowski J, Aimez V, Pauc N, Drouin D and Post M 2007a UV laser controlled quantum well intermixing in InAlGaAs/GaAs heterostructures *J. Phys.: Conf. Ser.* **59** 605

Genest J, Dubowski J J and Aimez V 2007b Suppressed intermixing in InAlGaAs/AlGaAs/GaAs and AlGaAs/GaAs quantum well heterostructures irradiated with a KrF excimer laser *Appl. Phys.* A **89** 423–6

Haysom J E, Delage A, He J J, Koteles E S, Poole P J, Feng Y, Goldberg R D, Mitchell I V and Charbonneau S 1999 Experimental analysis and modeling of buried waveguides fabricated by quantum-well intermixing *IEEE J. Quantum Elect.* **35** 1354–63

Helmy A S, Martin P, Landesman J P, Bryce A C, Aitchison J S and Marsh J H 2006 Spatially resolved photoluminescence and Raman spectroscopy of bandgap gratings fabricated in GaAs/AlAs superlattice waveguide using quantum well intermixing *J. Cryst. Growth* **288** 53–6

Hulko O, Thompson D, Czaban J and Simmons J 2006 The effect of different proximity caps on quantum well intermixing in InGaAsP/InP QW structures *Semicond. Sci. Technol.* **21** 870

Jie Z, Jie C, Yong-Chen W and De-Jun H 2006 Implant depth influence on InGaAsP/InP double quantum well intermixing induced by phosphorus ion implantation *Chin. Phys. Lett.* **23** 919–20

Kaleem M, Zhang X, Zhuang Y, He J J, Liu N and Dubowski J J 2013 UV laser induced selective-area bandgap engineering for fabrication of InGaAsP/InP laser devices *Opt. Laser Technol.* **51** 36–42

Kumar B and Soni R 2010 Synthesis of InP nanoparticles by pulsed laser ablation in ethanol *Mater. Chem. Phys.* **121** 95

Liu N, Blais S and Dubowski J J 2012 Surface and interface study of SiO_{2-x} coated InP/InGaAs/InGaAsP semiconductor laser microstructures processed in the soft KrF laser irradiation regime *Pacific Rim Laser Damage 2011: Optical Materials for High Power Lasers (Shanghai, China) Proc. SPIE* **8206** 820609

Liu N and Dubowski J J 2013 Chemical evolution of InP/InGaAs/InGaAsP microstructures irradiated in air and deionized water with ArF and KrF lasers *Appl. Surf. Sci.* **270** 16–24

Liu N, Moumanis K and Dubowski J J 2010 ArF excimer laser-induced quantum well intermixing in dielectric layer coated InGaAs/InGaAsP microstructures *Proc. PICALO 2010 (Wuhan, China)*

Liu N, Moumanis K and Dubowski J J 2012 Self-organized nano-cone arrays in InP/InGaAs/InGaAsP microstructures by irradiation with ArF and KrF excimer lasers *J. Laser Micro/Nanoeng.* **7** 130

McDougall S D, Kowalski O P, Hamilton C J, Camacho F, Qiu B C, Ke M L, De La Rue R M, Bryce A C and Marsh J H 1998 Monolithic integration via a universal damage enhanced quantum-well intermixing technique *IEEE J. Sel. Top. Quantum Electron.* **4** 636–46

Nie D, Mei T, Tang X, Chin M, Djie H and Wang Y 2006 Argon plasma exposure enhanced intermixing in an undoped InGaAsP/InP quantum-well structure *J. Appl. Phys.* **100** 046103

Noel J-P, Melville D, Jones T, Shepherd F, Miner C, Puetz N, Fox K, Poole P, Feng Y and Koteles E S 1996 High-reliability blue shifted InGaAsP/InP lasers *Appl. Phys. Lett.* **69** 3516–8

Ong T K, Gunawan O, Ooi B S, Lam Y L, Chan Y C, Zhou Y, Helmy A S and Marsh J H 2000 High-spatial-resolution quantum-well intermixing process in GaInAs/GaInAsP laser structure using pulsed-photoabsorption-induced disordering *J. Appl. Phys.* **87** 2775–9

Paquette M, Beauvais J, Beerens J, Poole P J, Charbonneau S, Miner C J and Blaauw C 1997 Blueshifting of InGaAsP/InP laser diodes by low-energy ion implantation *Appl. Phys. Lett.* **71** 3749–51

Singh R and Shewchun J 1978 A possible explanation for the photovoltaic effect in indium tin oxide on InP solar cells *J. Appl. Phys.* **49** 4588–91

Skogen E J, Raring J W, Morrison G B, Wang C S, Lal V, Masanovic M L and Coldren L A 2005 Monolithically integrated active components: a quantum-well intermixing approach *IEEE J. Sel. Top. Quantum Electron.* **11** 343–55

Stanowski R and Dubowski J J 2009 Laser rapid thermal annealing of quantum semiconductor wafers: a one step bandgap engineering technique *Appl. Phys.* A **94** 667–74

Sugg A, Chen E, Holonyak N, Hsieh K, Baker J and Finnegan N 1993 Effects of low-temperature annealing on the native oxide of $Al_xGa_{1-x}As$ *J. Appl. Phys.* **74** 3880–5

Teng J, Dong J, Chua S, Lai M, Foo B, Thompson D, Robinson B, Lee A, Hazell J and Sproule I 2002 Controlled group V intermixing in InGaAsP quantum well structures and its application to the fabrication of two section tunable lasers *J. Appl. Phys.* **92** 4330

Tsuchiya T, Komori M, Uomi K, Oka A, Kawano T and Oishi A 1994 Investigation of effect of strain on low-threshold 1.3 μm InGaAsP strained-layer quantum well lasers *Electron. Lett.* **30** 788–9

Xiang N, Tukiainen A, Dekker J, Likonen J and Pessa M 2001 Oxygen-related deep level defects in solid-source MBE grown GaInP *J. Cryst. Growth* **227–228** 244–8

Xu C and Mei T 2009 Inductively coupled argon plasma-enhanced quantum-well intermixing: cap layer effect and plasma process influence *IEEE J. Quantum Electron.* **45** 920–6

Zimmerman J A, Bach S B H, Watson C H and Eyler J R 1991 Ion/molecule reactions of arsenic and phosphorus cluster ions: ionization potentials and novel reaction pathways *J. Phys. Chem.* **95** 98–104